Spin-independent and spin-dependent conductance anisotropy in layered colossal-magnetoresistive manganite single crystals

Qing'An Li, K. E. Gray, and J. F. Mitchell
Materials Sciences Division, Argonne National Laboratory, Argonne, Illinois 60439
(Received 29 June 1998; revised manuscript received 26 October 1998)

Results are reported for the conductance anisotropies in single crystals of the layered colossal magnetoresistive manganites. Well below the magnetic ordering temperatures, the zero-field anisotropy increases from ~230 for $La_{1.24}Sr_{1.76}Mn_2O_7$ to >10 000 for $La_{1.4}Sr_{1.6}Mn_2O_7$, consistent with a *c*-axis antiferromagnetic ground state in the latter, while the *spin-independent* conductivity anisotropy only increases from ~230 to ~300. Significant *c*-axis ferromagnetic fluctuations are seen in $La_{1.4}Sr_{1.6}Mn_2O_7$, but no evidence is found for the recently reported two-dimensional magnetic ordering transition at higher temperatures. Direct evidence suggests that spin-orbit coupling is weaker than any other possible sources of orbital ordering.
[S0163-1829(99)11613-8]

INTRODUCTION

The collosal magnetoresistance (CMR) effect[1] is dramatic, both from the point of view of scientific interest and potential applications. Although a number of models[2–4] have been proposed to explain this phenomenon; there is no obvious consensus as to which, if any, of the models is correct. The recent discovery[5] of CMR in the layered manganites offers new opportunities to impact both our understanding of the phenomena and its potential applications. The large resistive anisotropy, resulting from the layered structure, can more decisively test models and the CMR effect is significantly larger.[5] However, the large anisotropy presents an interesting challenge to measure it properly, an issue shared by another class of highly anisotropic oxides, the high-temperature cuprate superconductors. In the latter case, the use of a six-terminal measurement,[6] rather than the customary four-terminal one, has proven to be quite insightful. Here, two variants of this are used to measure the in-plane (*ab*) and *c*-axis resistivities, ρ_{ab} and ρ_c, or conductivities, σ_{ab} and σ_c, simultaneously, and independently since this technique minimizes interference between them.

The temperature-dependent anisotropic conductances were determined in single crystals of $La_{1.24}Sr_{1.76}Mn_2O_7$ and $La_{1.4}Sr_{1.6}Mn_2O_7$ (hereafter referred to by their hole doping of 38% and 30%, respectively), which exhibit different magnetic order at low temperatures. Several results are reported: (1) the most significant difference is an increase of the low-temperature, zero-field anisotropy from ~230 for 38% to >10 000 for 30%, which is consistent with an antiferromagnetic (AF) *c*-axis ground state[7] in the latter; (2) the effects of spin and charge degrees of freedom on conductivity are isolated by aligning all spins to obtain the *spin-independent* conductivity, and its anisotropy, which only increases modestly, from ~230 for 38% to ~300 for 30%; (3) direct experimental evidence suggests that spin-orbit coupling is weaker than any other possible sources of orbital ordering; (4) with increasing temperature, the presence of significant *c*-axis ferromagnetic (FM) fluctuations from the AF ground state are found in the 30% sample; (5) below T_C, virtually identical temperature dependences for the spin-independent σ_{ab} and σ_c are found for *each* composition studied, consistent with the same conduction mechanism (e.g., double exchange), but the magnitude of $\rho_c \sim 0.5\,\Omega$ cm is unusually large for metallic conduction; and (6) no evidence is found for an in-plane, two-dimensional ordering transition,[7] as suggested by the observation[7] of a maximum in ρ_{ab} above the Curie temperature, T_C, for 30% doping, but we show how such qualitatively different temperature profiles can be *artifacts* of four-terminal measurements.

The first part of this paper includes a rather detailed account of the necessary experimental procedures to make definitive determinations of the principal parts of the conductance, which are presented subsequently. This is justified since these procedures are not universally followed, but by ignoring them there is a potential to reach quantitatively, and even qualitatively, wrong conclusions.

SAMPLE FABRICATION AND CHARACTERIZATION

Crystals of the 30% and 38% materials were melt grown in flowing 20% O_2 (balance Ar) using a floating-zone optical image furnace (NEC Model SC-M15HD). Samples for the measurements described in this work were cleaved from the resulting polycrystalline boules.[8] The relative widths of zero-field transitions are likely one of the best indicators of crystal quality. It is hard to imagine that any imhomogeneity or other inferior aspect of a sample's quality would produce a sharper transition. All the samples reported here exhibit the sharpest reported transition widths and minimal evidence of inhomogeneities, using tests described below.

TRANSPORT MEASUREMENTS

For electrical contacts, Au was sputtered onto the *c*-axis-normal surfaces in a pattern of stripes perpendicular to the long dimension of the crystal. Four stripes were placed symmetrically on both the top and bottom surfaces. In the standard six-terminal configuration, the outer stripes on the top surface supply the current, *I*. Then the inner stripes on that surface define $V_{\rm top}$ and the inner stripes on the bottom surface, $V_{\rm bot}$ [see Fig. 1(a)]. Samples were measured in a stan-

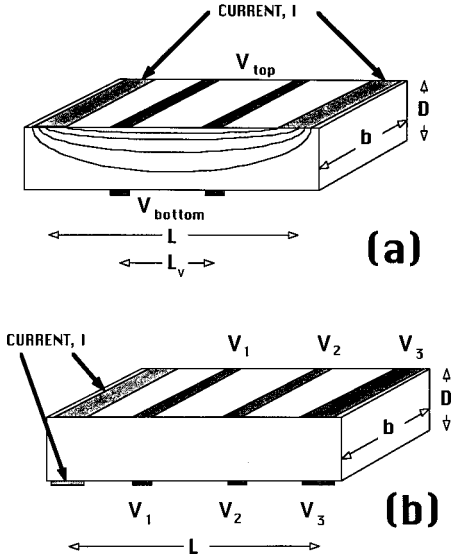

FIG. 1. Schematic diagram of samples with current and voltage contacts for the two configurations used here.

dard ^{4}He gas flow cryostat. Heating was avoided by reducing the current, and hysteresis, caused by slight thermometer-sample temperature differences, was avoided by sweeping the temperature slowly, especially near the transition.

The starting point for the analysis of Ref. 6 is only valid for linear current-voltage characteristics, as is the case for these CMR crystals. To obtain sufficient accuracy, crystals must exhibit very uniform properties (ρ_{ab} and ρ_c), be free of even low-angle grain boundaries (mosiac) and be close to a rectangular-parallelepiped shape. It is also necessary to extend the analysis of Ref. 6 beyond the first term in the series solution of Laplace's equation for the potential.[9] For high values of the anisotropy, ρ_c/ρ_{ab}, the complete series solution can be approximated by:

$$V_{\rm top}\sim (l/b)\sqrt{\rho_{ab}\rho_c}C_0\{1+C_1\exp(-2\pi D\xi/L)+\text{h.o.t.}\}, \tag{1}$$

$$V_{\rm bot}\sim \frac{(l/b)\sqrt{\rho_{ab}\rho_c}}{\sinh(\pi D\xi/L)}D_0\{1+D_1\exp(-2\pi D\xi/L)+\text{h.o.t.}\} \tag{2}$$

(h.o.t. ≡ higher order terms) where $\xi=\sqrt{\rho_c/\rho_{ab}}$, L is the length in the current direction, b the width, and D the thickness top to bottom (see also Ref. 9). The current density falls off exponentially with distance from the top surface [Eq. (2)] with a characteristic length $D_{\rm eff}$:

$$D_{\rm eff}=\frac{L}{\pi}\sqrt{\rho_{ab}/\rho_c}, \tag{3}$$

which is temperature dependent and typically ~3–40 μm for the crystals used here.

Although the C and D coefficients are somewhat clumsy expressions and integrals which are evaluated numerically, it is relatively straightforward to include the experimentally measured contact widths and locations, even if they are not all symmetrically placed (e.g., $V_{\rm top}$ and $V_{\rm bot}$). For sufficiently large $D\xi/L$, both C_1 and D_1 can be neglected so that $\sqrt{\rho_{ab}\rho_c}$ is determined from $V_{\rm top}$ and $\xi=\sqrt{\rho_{ab}/\rho_c}$ is determined from $V_{\rm top}/V_{\rm bot}$. However, if $D\xi/L$ is too large, $V_{\rm bot}$ cannot be measured above system noise and *only* $\sqrt{\rho_{ab}\rho_c}$ is determined. In this case, a second multiterminal variant [see Fig. 1(b)] is useful. Current is injected from the top to bottom surfaces (at one end of the crystal) and the voltages measured using at least two pairs of top to bottom contacts. Although the analysis involves more complex expressions, it also determines ρ_{ab} and ρ_c individually from the ratios of such voltages. Note that for very large anisotropy, the ratio is one and only ρ_c is measured.

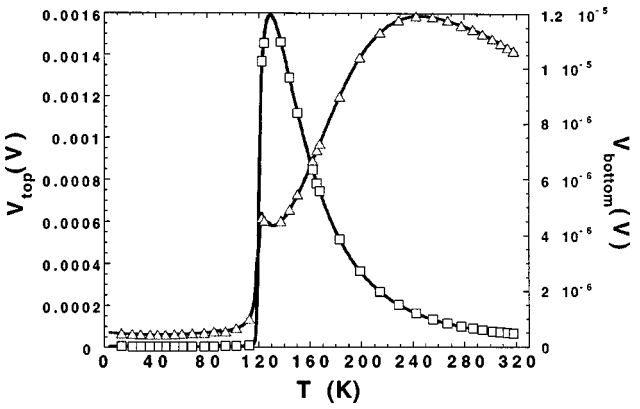

FIG. 2. As input to Eqs. (1) and (2), the measured $V_{\rm top}$ (squares) and $V_{\rm bot}$ (triangles) are displayed as a function of temperature for a 38% crystal with current (10 μA) injected in the top, outer electrodes [see Fig. 1(a)].

These multiterminal configurations allow several crucial tests of crystal uniformity (e.g., doping). First, comparisons can be made for current injected into the outer stripes on the *bottom surface* [see Fig. 1(a)]. For the variant shown in Fig. 1(b), voltage ratios are compared for current injection at opposite ends of the crystals. These tests readily validate the uniformity of our best crystals used here.

The measured $V_{\rm top}$ and $V_{\rm bot}$ on a 38% crystal are shown in Fig. 2 as a function of temperature ($I=10\,\mu$A, $D=0.13$ mm). Analysis of this data is shown in Fig. 3 as ρ_{ab} and ρ_c with a low-temperature anisotropy of ~230. The tem-

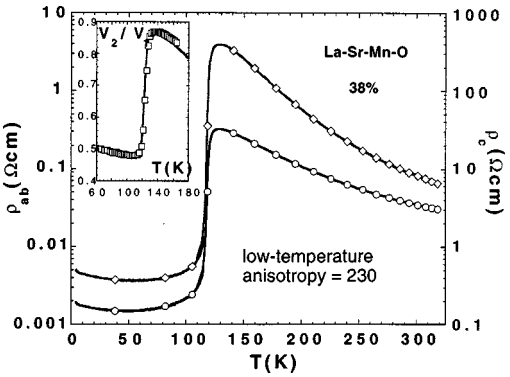

FIG. 3. Principle parts of the anisotropic resistivity, ρ_{ab} (circles) and ρ_c (diamonds), as derived from the data of Fig. 2 for a 38% crystal using Eqs. (1) and (2). The low-temperature anisotropy is close to 230. Inset: an example in a 40% crystal of the measured voltage ratio (squares) for the setup of Fig. 1(b) compared with the calculated ratio (solid line) based on ρ_{ab} and ρ_c from the setup of Fig. 1(a).

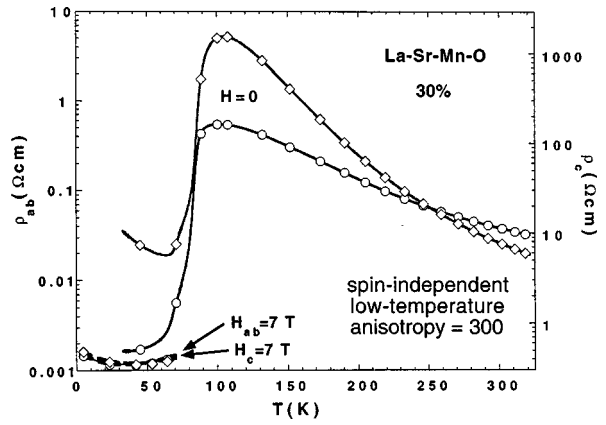

FIG. 4. The principle anisotropic resistivities, ρ_{ab} (circles) and ρ_c (diamonds), as derived from data on a 30% crystal using Eqs. (1) and (2). Note the insulating behavior of ρ_c below T_C. Data in applied fields of 7 T, both parallel to the *c* axis (diamonds and circles) and *ab* plane (dashed lines), reproduce the general shapes found for the 38% crystal in zero field and define a spin-independent anisotropy of 300.

perature profile of V_{bot} can be understood by realizing that the current flows along both the *c* axis and *ab* planes in series. Just above T_C, ρ_c peaks more sharply than ρ_{ab}. As such, the current to V_{bot} decreases, but also most of the voltage drop is along the *c* axis and not between the electrodes of V_{bot}. Thus any data in anisotropic manganites which is qualitatively similar to V_{bot} of Fig. 2, e.g., that of Ref. 7, must be treated with suspicion as a possible artifact of slight contact misalignment ($\sim$0.1 mm).

One important test of the analysis and of crystal uniformity is obtained by measuring the voltage ratios for the configuration of Fig. 1(b), e.g., V_2/V_1. These are compared to calculated ratios using ρ_{ab} and ρ_c from an analysis of the configuration of Fig. 1(a). The typically excellent agreement is shown in the inset to Fig. 3 for a 40% crystal. A simple ultimate test of the procedure is to substitute the calculated values of ρ_{ab} and ρ_c into the *complete* series solution for V_{top} and V_{bot} and compare them to the measured ones. In doing so, the terms beyond C_0 and D_0 in Eqs. (1) and (2) were found to be most important where the anisotropy is smallest (e.g., for $T > T_C$) and for the 30% sample (see below). However, using only C_0 and D_0, the discrepancy in V_{top} (V_{bot}) for the 30% crystal is less than 1% (0.1%) below T_C, rising to $\sim$5% (0.3%) at room temperature as the anisotropy falls. Including C_1 and D_1 reduced these discrepancies to 10^{-7}% (10^{-5}%) below T_C, rising to $\sim$0.0003% (0.004%) at room temperature. The correction terms were about an order of magnitude smaller for the 38% sample. The data analyzed in this paper included the C_1 and D_1 terms.

RESULTS

In addition to the results for a 38% sample shown in Fig. 3, the calculated resistivities for a 30% crystal ($D = 0.1$ mm) are shown in Fig. 4. The low-temperature behavior of the resistivity and T_C of this 30% crystal is very similar to other reports[7,10] but this transition width is much narrower. One feature is the large anisotropy which surpasses 10 000 below 30 K. As a result of this, V_{bot} drops below the voltmeter noise so the calculated ρ_{ab} and ρ_c (not shown) display identical temperature dependences coming from V_{top} which, from Eq. (1), approximates $\sqrt{\rho_{ab}\rho_c}$. Below 30 K, data for the geometry of Fig. 1(b) is needed to separate ρ_{ab} and ρ_c. These indicate that the anisotropy and ρ_c continue to increase while ρ_{ab} approximates the temperature dependence of the 38% sample. The increasing ρ_c as temperature decreases is consistent with a *c*-axis AF ground state.[7]

A second feature is the lack of evidence for the proposed[7] two-dimensional magnetic ordering transition well above T_C for 30% doping which was based on an observation[7] of a maximum in ρ_{ab} above the Curie temperature, coupled with in-plane magnetization data.[10] By comparing their data[7] to V_{bot} of Fig. 2, we note that such a qualitatively different temperature profile above T_C can be an *artifact* of four-terminal measurements if the contacts are slightly misaligned along the *c* axis. The magnetization data[10] are similar in magnitude ($\sim$1%) and temperature dependence (above T_C) to that found[8] in 40% samples which have never exhibited a high-temperature maximum in ρ_{ab}. This data was explained[8] by the presence of crystal intergrowths of multiple Mn-O layers, seen by TEM, which approximate the higher-T_C perovskite. In distinct contrast to the behavior at the bulk T_C, the magnetization[10] rises much more sharply than ρ_{ab} drops, confirming that these have different origins. Note also that the drop of the *in-plane* magnetization[10] below the bulk T_C by a factor of two may be due to magnetic coupling of the intergrowths to the *out-of-plane* AF ordering of the spins in bulk, layered 30% material, whereas for 40%, the spontaneous in-plane FM ordering is identical to the intergrowth magnetic order.[8]

Although the conductivities depend strongly on the spin order, it is both possible and useful to isolate the effects of spin and charge degrees of freedom on the conductivity by aligning all spins to obtain the *spin-independent* conductivity and its anisotropy from measurements of ρ_{ab} and ρ_c in the (nearly) saturated FM state. The spontaneous FM ordering in both the basal planes and along the *c* axis for the 38% sample closely approximates such saturation below T_C and defines an anisotropy of 230 (see Fig. 3). For the AF *c*-axis ordering in the 30% crystal it is necessary to apply a large field to align the spins. Data at 7 T (shown in Fig. 4 for both *c*-axis and basal plane directions) indicate a *spin-independent* anisotropy of 300 for the 30% sample, i.e., close to the 38% sample. Note that the independence of ρ_{ab} and ρ_c on field direction, shown in Fig. 4 at 7 T, proves that the *c*-axis conductivity depends only on the *relative* nearest-neighbor spin orientation and not on absolute spin orientation, e.g., the projection along the *c* axis. Since the occurrence of orbital ordering, or changes in it, would certainly be expected to affect transport in the manganites, the virtually complete independence of ρ_{ab} and ρ_c on spin direction provides direct evidence that spin-orbit coupling is weaker than any other possible sources of orbital ordering.

The effects of magnetic order on transport are more directly seen in the conductivity, i.e., σ_{ab} and σ_c. These are shown in Fig. 5 for the 38% and 30% crystals with σ_c scaled by the spin-independent anisotropies. The zero-field temperature dependences just below T_C are fit to the scaling form $\sigma_{ab} \sim (1 - T/T_C)^m$, where $m \sim 0.33 - 0.35$. An empirical correspondence[11] with the zero-field, local magnetization M

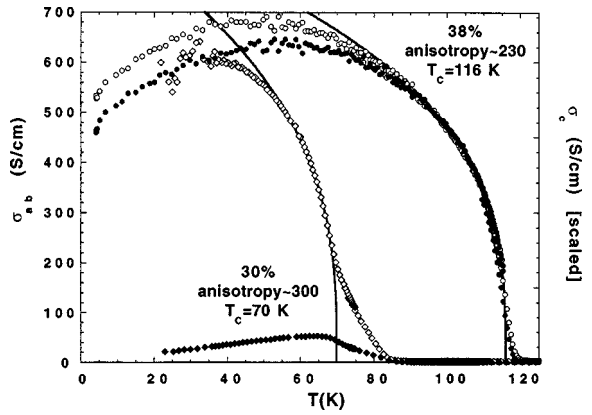

FIG. 5. The principle parts of the anisotropic conductivities σ_{ab} and σ_c for both the 30% (open and filled circles) and 38% (open and filled diamonds) crystals from the data of Figs. 3 and 4. In each case, σ_c is scaled by the low-temperature spin-independent anisotropy, i.e., 300 and 230, respectively. Solid lines are fits to the scaling function, $\sigma \sim (1-T/T_C)^m$, just below T_C, are shown to define T_C as 70 and 116 K, respectively.

revealed from neutron scattering for a 40% sample, indicates that $\sigma \sim M^2$, and this extends into the apparent fluctuation regime just above the fit values of T_C. The similar scaling for the 38% and 30% crystals implies this is a general property.

At sufficiently high temperatures both ρ_{ab} and ρ_c appear to be thermally activated with constant activation energies. Arhennius plots yield activation energies which are summarized in Table I, together with the other parameters describing these materials. Except for the effects of the AF ground state of the 30% crystal, the properties and anisotropies are only modestly dependent on doping. However, the decrease in σ_{ab} at low temperatures is inconsistent with usual metallic conductivity and conventional magnetic order. While it can be fit by variable-range hopping, the temperature interval is too narrow to confirm this mechanism nor to distinguish its dimensionality. Others[12] have made convincing fits to $\sigma_0 + A\sqrt{T}$ down to 30 mK, which closely match our lowest-temperature data. This behavior is expected for a highly disordered, three-dimensional metal.

The issue of metallic conductivity is also addressed by another aspect of the data. Below T_C, the virtually identical temperature dependences of σ_{ab} and σ_c seen in Fig. 5 for the 38% crystal (and at 7 T for the 30% crystal in Fig. 4) imply that the mechanisms of *c*-axis and *ab*-plane conductance are the same. This is consistent with the double-exchange mechanism, since the *spin-independent* conductance anisotropy can merely reflect the greater Mn-Mn distance for the double-exchange process along the *c* axis. But it is also a nontrivial result since such a large resistivity as $\rho_c \sim 0.5\,\Omega$ cm would be highly unusual for metallic conductivity. For this large ρ_c to be a valid concern requires ruling out a second suggested explanation of the virtually identical temperature dependences of σ_{ab} and σ_c.

TABLE I. Compendium of parameters determined for the layered manganites.

Single crystal composition	30%	38%
T_C	70 K	116 K
m (scaling exponent)	0.35	0.33
Low-T anisotropy	>10 000	230
ρ_{ab} (~40 K, zero field)	1.7 mΩ cm	1.4 mΩ cm
Low-T spin-independent anisotropy	300	230
High-T *c*-axis activation energy	~1570 K	1200 K
High-T *ab*-plane activation energy	~710 K	700 K

The alternative explanation suggests that the *c*-axis current path could include current flow along the *ab* planes which are bridged by occasional shorts occurring *between* Mn-O bilayers. While this would affect the configuration of Fig. 1(b), the analysis of Fig. 1(a) already includes *ab*-plane transport. However, it cannot distinguish between uniform *c*-axis conductance or occasional shorts unless their spacing approaches the distance between contacts since inhomogeneities on that distance scale are ruled out by the highly consistent multiple tests [i.e., both Fig. 1(a) and 1(b) and in each case by exchanging current contacts from one side of the crystals to the other] and otherwise the solution of Laplace's equation would be invalid. Thus this scenario *requires* a high density of shorts. However, a critical flaw in this scenario may be its inability to simply explain the significantly different temperature dependences of ρ_{ab} and ρ_c seen for $T > T_C$ in Figs. 3 and 4. The internal consistency of this scenario requires that for $T < T_C$, the effective ρ_c' is proportional to $\rho_{ab}(T)$, and that for $T > T_C$, the contribution of the shorts to ρ_c' is less than that of the intrinsic ρ_c. For illustration, two limiting cases for the resistivity of the shorts ρ_s are considered: (1) $\rho_s(T) = \beta \rho_{ab}(T)$; and (2) $\rho_s = \rho_0$, where β and ρ_0 are constants. Using experimental values for the 38% sample, simple considerations imply for (1) that β must be $\ll 1$, and for (2) that the mean distance between shorts, l, is $\gg 1$ micron. Neither is impossible, but both stretch our sense of credibility (in the latter case, since l approaches the distance between contacts). Also, there is no evidence in either conventional nor high-resolution transmission electron microscopy[13] for defects which could satisfy such a scenario. We conclude that it is highly unlikely that interbilayer shorts can explain the similar spin-independent σ_{ab} and σ_c below T_C.

Two other features of the conductivity for the 30% sample need understanding: (1) the apparent minority component of FM order along the *c* axis, as evidenced by the significant value of σ_c in the vicinity of T_C, and (2) the exaggerated ''foot'' of the transition above T_C. Although the σ_c contribution below T_C could be due to a competition between AF superexchange and double exchange or due to a FM impurity phase (e.g., different doping), its disappearance at low temperatures would then be hard to understand and it is seen universally.[7,10] Instead, the linear temperature dependence of σ_c, found by using our methods, is highly suggestive of a fluctuation effect, which is consistent with the observation in a 40% crystal of very soft, *c*-axis spin waves[14] and the similarly small interbilayer exchange coupling constant found in our 30% crystal.[15] The data for the 30% crystal strongly suggest the existence of significant *c*-axis FM-like fluctuations from the AF ground state in the vicinity of T_C. While the foot above T_C may be caused by sample inhomogeniety, it is also seen universally by us and by others[7,10] and for each composition. Our comparisons, de-

scribed above, using different lead configurations imply that any inhomogeneities must be on a microscopic length scale.

SUMMARY

The principal parts of the zero-field anisotropic conductivity σ_{ab} and σ_c are determined as a function of temperature for two compositions of the layered manganites $La_{1.24}Sr_{1.76}Mn_2O_7$ and $La_{1.4}Sr_{1.6}Mn_2O_7$. These data show qualitative differences below T_C in the anisotropy (230 and $>10\,000$, respectively) and in the field dependence which is only strong in the latter. However, the *spin-independent* anisotropy only increases from $\sim$230 to $\sim$300, and direct experimental evidence suggests that spin-orbit coupling is weaker than other possible sources of orbital ordering. Above T_C, both ρ_{ab} and ρ_c are thermally activated and it is clear that ρ_{ab} and ρ_c for 30% doping (Fig. 4) display qualitatively similar temperature profiles to the 38% sample. The qualitatively different temperature profile reported recently[7] for 30% crystals is not reproduced here. Although the differences could be due to crystal quality (e.g., doping), our crystals exhibit significantly narrower transitions. Since the data of Ref. 7 resembles $V_{\rm bot}$ of Fig. 2, it could also be due to a small misalignment ($\sim$0.1 mm) along the *c* axis of voltage and current contacts. As such, the conclusion[7] of two-dimensional magnetic order significantly above T_C is called into question. Data for the 30% crystal strongly suggest the existence of significant *c*-axis FM-like fluctuations in the vicinity of T_C. Finally, suggestions of metallic conductivity below T_C requires an understanding of the very small magnitude of σ_c for 38%, which exhibits the same temperature dependence as σ_{ab}.

ACKNOWLEDGMENTS

The authors thank Paul Paulikas for technical assistance and acknowledge useful discussions with Ray Osborn, Stefan Rosenkranz, Sam Bader, Michael Norman, and Dean Miller. This research was supported by the U.S. Department of Energy, Basic Energy Sciences-Materials Sciences, under Contract No. W-31-109-ENG-38.

[1] S. Jin, T. H. Tiefel, M. McCormack, R. A. Fastnacht, R. Ramesh, and L. H. Chen, Science **264**, 413 (1994).
[2] C. Zener, Phys. Rev. **82**, 403 (1951); P. W. Anderson and H. Hasegawa, *ibid.* **100**, 675 (1955); P. G. de Gennes, *ibid.* **118**, 141 (1960).
[3] A. J. Millis, P. B. Littlewood, and B. I. Shraiman, Phys. Rev. Lett. **74**, 5144 (1995).
[4] W. E. Pickett and D. J. Singh, Phys. Rev. B **53**, 1146 (1996).
[5] Y. Moritomo, A. Asamitsu, H. Kuwahara, and Y. Tokura, Nature (London) **380**, 141 (1996).
[6] R. Busch, G. Ries, H. Werthner, G. Kreiselmeyer, and G. Saemann-Ischenko, Phys. Rev. Lett. **69**, 522 (1992).
[7] T. Kimura, Y. Tomioka, H. Kuwahara, A. Asamitsu, M. Tamura, and Y. Tokura, Science **247**, 1698 (1996).
[8] J. F. Mitchell, D. N. Argyriou, J. D. Jorgensen, D. G. Hinks, C. D. Potter, and S. D. Bader, Phys. Rev. B **55**, 63 (1997).
[9] G. A. Levin, J. Appl. Phys. **81**, 714 (1997).
[10] T. Kimura, A. Asamitsu, Y. Tomioka, and Y. Tokura, Phys. Rev. Lett. **79**, 3720 (1997).
[11] R. Osborn, S. Rosenkranz, D. N. Argyiou, L. Vasiliu-Doloc, J. W. Lynn, S. K. Sinha, J. F. Mitchell, K. E. Gray, and S. D. Bader, Phys. Rev. Lett. **81**, 3964 (1998).
[12] Y. Tokura (private communication).
[13] D. J. Miller (private communication).
[14] S. Rosenkranz, R. Osborn, L. Vasiliu-Doloc, J. W. Lynn, S. K. Sinha, and J. F. Mitchell (private communication).
[15] Qing'An Li, K. E. Gray, J. F. Mitchell, A. Berger, and R. Osgood (private communication).